Precambrian Research 350 (2020) 105878

Contents lists available at ScienceDirect

Precambrian Research

journal homepage: www.elsevier.com/locate/precamres

Insights into the processes and controls on the absolute abundance and distribution of manganese in Precambrian iron formations

Mehrnaz Siahi[a], Harilaos Tsikos[a,*], Sipesihle Rafuza[a], Paul B.H. Oonk[a], Xolane R. Mhlanga[a], Deon van Niekerk[a], Paul R.D. Mason[b], Chris Harris[c]

[a] Geology Department, Rhodes University, Makhanda/Grahamstown 6140, South Africa
[b] Department of Earth Sciences, Utrecht University, Princetonlaan 8A, 3584CB, the Netherlands
[c] Department of Geological Sciences, University of Cape Town, Rondebosch 7700, South Africa

ARTICLE INFO

Keywords:
Iron formation
Carbonates
Manganese
GOE
Diagenesis

ABSTRACT

The role of manganese as redox tracer in the context of iron formations (IF) has received renewed attention in recent years. The utility of several redox-sensitive trace metal proxies in IF (*e.g.,* Mo) is based on the premise that simultaneously elevated manganese concentrations in the form of primary Mn(IV) oxides, would have controlled the redox behaviour and stable isotope variations of such elements during primary deposition and diagenesis. Recent research on the mineral fraction-specific geochemistry of Paleoproterozoic IF from South Africa (Griquatown and Kuruman Iron Formations) reports no preserved Mn(IV) oxides and a strong affinity of manganese (> 90%) to partition into carbonate minerals as Mn(II). In this study, we exploit further this relationship by examining in detail the mineral-specific abundance and distribution of manganese across the same IF succession, with main emphasis on the Mn-enriched upper 120 m of the Griquatown IF. Dominant carbonate minerals include ankerite, siderite and occasional calcite, with MnO contents across all three minerals ranging from less than 1 to well over 10 wt%. Co-existing ankerite and siderite on the scale of individual thin sections record very similar MnO (and MgO) contents at statistically very low variance. Calcite is only observed as relic phase showing apparent textural evidence for replacement by ankerite and siderite. The calcite is Mg-rich (up to 15 wt % MgO) and contains the highest MnO contents out of the entire dataset obtained. Variability in the MnO content of calcite is also high and anti-correlates strongly with CaO content. Ankerite and siderite co-existing with calcite have similar MnO and MgO concentrations, consistent with conservative transfer during replacement reactions and only net addition of Fe(II) from pore fluids. For one of the calcite-containing samples, all three carbonate minerals were also analysed sequentially for carbon isotopes and yielded very similar $\delta^{13}C$ values (−6.7 to −6.0‰). We interpret the above features as indicative of primary calcite being the dominant mode of manganese acquisition in the initial sediment. Diagenetic replacement reactions then homogeneously reworked Mn (along with Mg and Ca) in a largely conservative fashion into diagenetic ankerite and siderite. Our interpretation questions IF models that assume high primary Mn(IV) oxide deposition and its bacterially-mediated diagenetic reconstitution in IF during transient oxygenation events (oxygen "whiffs"); instead, it lends support to emerging ideas for primary water-column processes leading to the formation and precipitation of reduced Fe(+Mn) mineral species as precursors to IF.

1. Introduction: defining manganese-rich iron formation

The behaviour of manganese during deposition of iron formations (IF) has historically been a topic of fluctuating interest. In general, IF are known to be rocks with very low bulk manganese concentrations relative to those of iron (Klein, 2005). These low abundances, combined with the mono-isotopic character of manganese, compound its generally low appeal as a redox proxy of choice for deciphering the origin of IF. To this end, a striking exception is the giant carbonate-rich sedimentary manganese deposits of the Kalahari Manganese Field in South Africa (Tsikos et al., 2003, 2010): these constitute a world-class resource of manganese, hosted within the Hotazel IF, and have previously been interpreted to have formed as a result of increased oxidative conditions in the aftermath of the Great Oxidation Event (GOE) and Huronian-age global glaciation (Kopp et al., 2005). Even in this specific case, however, the distribution of manganese between the host

* Corresponding author.
E-mail address: h.tsikos@ru.ac.za (H. Tsikos).

https://doi.org/10.1016/j.precamres.2020.105878
Received 15 December 2019; Received in revised form 19 June 2020; Accepted 22 July 2020
Available online 27 July 2020

Hotazel IF and the Mn-rich layers themselves is strongly biased, with contents in the former being very low and thus comparable to other IF elsewhere (Tsikos et al., 2003).

Earlier studies attributed the dearth of manganese in IF to processes of UV-induced marine deposition of Fe(III) oxyhydroxides and concomitant exclusion of Mn(IV) oxides from the precursor sediments (Anbar and Holland, 1992). The advent of biological models for IF deposition has ruled out UV radiation as a major driver for primary iron precipitation (Konhauser et al., 2002, 2005, 2017), leading to alternative mechanisms for the occasionally high manganese in IF to be proposed. These essentially interpret manganese enrichments in IF as a result of episodic primary precipitation of Mn(IV) oxides that ensued under oxidative maxima caused by transient bursts of photosynthetic dioxygen production (oxygen "whiffs"; Anbar et al., 2007). The manganese oxides are thought to have controlled the redox behaviour of, and related isotopic fractionation effects (where relevant) for a number of trace metals (Mo, Co, Tl), and would have shuttled these signals to the primary sediments (*e.g.*, Planavsky et al., 2014; Kurzweil et al., 2016; Ostrander et al., 2019). Quantitative sequestration of the initial precipitates into reduced mineral species (such as carbonates) *via* diagenetic transformations, would have led to effective preservation of the primary isotopic signatures.

Recent data from IF in South Africa (Oonk et al., 2017) have revealed that manganese is almost exclusively (> 90%) contained in the carbonate mineral fraction. This is in overall agreement with previous reports of unmetamorphosed, Mn-enriched IF in the literature (Johnson et al., 2013b; Kurzweil et al., 2016). It follows that the bulk-rock content of manganese in IF would be dictated by two combined factors: the modal abundance of carbonate minerals in a given sample; and the composition of the contained carbonate phases with respect to Mn *versus* other typically carbonate-hosted cations (Fe, Mg, Ca). At the same time, IF is a very heterogeneous rock with banding/layering manifested through a plethora of mineralogical combinations on all scales. Therefore, whether a bulk IF can be characterised as Mn-rich or Mn-poor, will always be dependent on the analysed sample size of that IF against its intrinsic textural heterogeneity.

The definition of manganese enrichment in IF is also dependent upon the geochemical context for comparative considerations: if the chosen reference is that of average crust (Fe/Mn = 50:1) then, in principle at least, values lower than the crustal ratio would correspond to a Mn-enriched IF. In terms of carbonate chemistry, an Fe/Mn ratio of 50:1 would correspond very closely to an average of 1.2 wt% MnO in $FeCO_3$ (siderite), or to 0.4 wt% MnO in $Ca(Fe,Mg)(CO_3)_2$ (ankerite) with an average FeO content of 20 wt%. In order to overcome the nuances of mineralogical control on the Fe/Mn ratio in IF (*i.e.*, variations in modal mineralogy, relative abundance of carbonates and their mineral-specific compositional variabilities), we hereby propose the carbonate-hosted Fe/Mn ratio as the one representing relative manganese endowment in IF. Such a convention would assist in removing the problem of sampling bias that all IF typically present: simply speaking, a sample of a given IF confined to a single carbonate-bearing chert band would arguably contain the (relatively) lowest Fe/Mn ratio and thus highest possible relative Mn content. Conversely, a sample from the same IF incorporating a carbonate-rich chert band and (at least part of) adjacent magnetite-dominated bands, would return a much higher "bulk-rock" Fe/Mn ratio, due to dilution of the corresponding carbonate-specific ratio by incorporation of Mn-lean magnetite (Fe_3O_4).

The above disparity is fittingly illustrated in Fig. 1 which presents a compilation of stratigraphically-controlled, MnO concentration data for bulk samples and their corresponding carbonate fractions from the Asbestos Hills Subgroup of South Africa (Kuruman and Griquatown IF). The diagram displays not only consistently lower bulk-rock MnO contents compared to carbonate-specific ones (in wt%), but also above-crust manganese enrichments in the uppermost 120 m of the Griquatown IF, with bulk carbonate-hosted MnO contents higher than the value of 2 wt% for approximately 50% of the total sample population. Against a whole-rock average FeO value of 32.2 ± 9.2 wt% across the entire Asbestos Hills sequence (Oonk et al., 2017), the specific stratigraphic interval above may be regarded as one of the most sustained records of increased Mn deposition in the context of global pre-GOE IF. In summarising, for the purposes of this paper we will consider the carbonate-specific manganese abundance in defining its relative concentration in any given sample of IF.

1.1. Origin of carbonate minerals in IF

Dominant carbonate minerals in IF are the Fe-rich species ankerite and siderite; by contrast, Fe-poor, Ca-Mg carbonates (calcite, dolomite) are very uncommon (*e.g.,* Gole and Klein, 1981; Baur et al., 1985; Beukes and Klein, 1990; Kaufman et al., 1990; Tsikos and Moore, 1997; Klein, 2005; Haugaard et al., 2016). Prevailing interpretations for the origin of iron carbonates in IF propose an exclusively diagenetic origin *via* microbially-mediated dissimilatory iron reduction (DIR; Fröelich et al., 1979; Walker, 1984; Nealson and Myers, 1990). DIR models predict that siderite and ankerite would have formed by coupled reduction of ferric iron supplied to the sediment, chiefly in the form of primary ferrihydrite, in contact with organic matter as the electron donor (Johnson et al., 2003, 2005; Konhauser et al., 2005, 2017; Heimann et al., 2010; Johnson et al., 2013a; Posth et al., 2013). Common derivation of organic carbon and Fe(III) oxyhydroxides may have been possible through processes of photoferrotrophy, oxidation of Fe(II) by molecular oxygen produced by cyanobacteria, or combinations thereof.

The basic reaction (1) below describing DIR, predicts that four moles of ferrihydrite will be reduced by a mole of organic carbon (expressed simplistically as CH_2O). The products of such reaction will be one mole of CO_2 representing re-mineralised organic C, and four moles of Fe(II):

$$CH_2O + 4Fe(OH)_3 + 8H^+ \rightarrow CO_2 + 4Fe^{2+} + 11H_2O \quad (1)$$

The delivery of carbonate alkalinity and Fe(II) through reaction (1), predicts *in situ* siderite formation with a $\delta^{13}C$ value approximating that of the reacting organic matter, provided that the system is closed with respect to carbon. The excess Fe(II) production following siderite formation through reaction (1), is interpreted to have given rise to other reduced or mixed valence iron minerals that typically occur in IF, such as Fe silicates (*e.g.,* minnesotaite) and/or magnetite (Heimann et al., 2010).

It should be noted that the simple DIR reaction (1) above constitutes the exact reverse reaction (2) below representing photoferrotrophy (Crowe et al., 2008; Konhauser et al., 2017):

$$4Fe^{2+} + CO_2 + 11H_2O \rightarrow CH_2O + 4Fe(OH)_3 + 8H^+ \quad (2)$$

Combination of reactions (1) and (2) suggests that the bulk oxidation state of iron in IF ought to be very close to 2, should photoferrotrophy and DIR have been the two sole mechanisms of iron redox cycling in the IF ocean, and diagenetic ferrous mineral formation from the original ferric precursors was quantitative. Global IF have an average Fe oxidation state of ~2.4 (Klein, 2005) and therefore contain excess Fe(III), primarily through the abundance of magnetite. Consequently, it is possible that either DIR took place in an open diagenetic environment with respect to iron and carbon (see also Thompson et al., 2019), or that processes of ferric mineral formation in IF were at least partly decoupled from the combined effects of photoferrotrophy and DIR.

1.2. Manganese in IF in the context of carbonate formation

As also indicated earlier, current thinking posits primary manganese deposition in IF in the form of tetravalent Mn oxides as a result of transient events of increased oxygenation (oxygen whiffs; Anbar et al., 2007). An additional inference assumes that, at times of maximum Mn

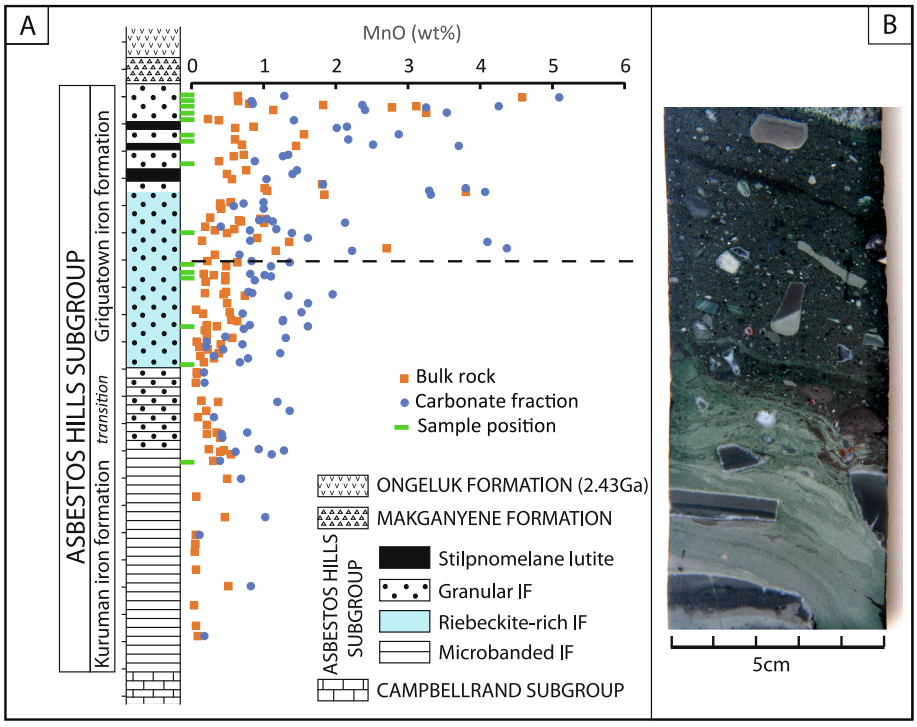

Fig. 1. A. Stratigraphic variability in whole-rock and carbonate-specific manganese abundances (both expressed as wt% MnO) across the Asbestos Hills Subgroup of the Transvaal Supergroup in the Northern Cape Province of South Africa (Kuruman and Griquatown Iron Formations). The horizontal dashed line denotes the stratigraphic level above which carbonate-specific MnO contents exceed the value of 2 wt% for approximately 50% of the corresponding data population. Stratigraphic position of 15 of the 16 samples (sample HOT from the Hotazel Formation is not displayed) selected for this study are indicated in green markers. Stratigraphically adjacent lithologic entities to the Asbestos Hills Subgroup are also shown, namely overlying diamictite of the Makganyene Formation and andesitic volcanic rocks of the Ongeluk Formation (lower Postmasburg Group), and underlying carbonate rocks of the Campbellrand Subgroup. The vertical scale of the stratigraphic column is only approximate, at an interval of 20 m. The 2.43 Ga age for the Ongeluk Formation is sourced from the paper of Gumsley et al. (2017). Adapted from Oonk et al. (2017). B. Photographic image of the evidently conformable nature of the lithologic contact between the uppermost Griquatown IF (below) and the Makganyene diamictite (above), as captured in drillcore HEX (see also Fig. 2 for precise locality). Note the apparent soft-sediment deformation effect of Makganyene dropstones draped in silicate facies Griquatown IF. (For interpretation of the references to colour in this figure legend, the reader is referred to the web version of this article.)

(IV) supply to the primary sediment, organic matter and Fe(III) species would have continued to co-precipitate. Microbially mediated, dissimilatory redox reactions involving both metal oxides of Mn(IV) and Fe (III) with organic carbon, would have prevailed during diagenesis. On the basis of standard thermodynamic principles and field observations in extant anaerobic diagenetic environments (Fröelich et al., 1979; Myers and Nealson, 1988; Nealson and Myers, 1990), dissimilatory Mn (IV)-reduction (DMR) would have sequentially preceded Fe(III)-reduction (*i.e.,* DIR) through the reaction:

$$CH_2O + 2MnO_2 + 4H^+ \rightarrow CO_2 + 2Mn^{2+} + 3H_2O \quad (3)$$

Reaction (3) above, theoretically predicts that two moles of the original MnO_2 would lead to the formation of one mole of pure end-member $MnCO_3$, while simultaneously delivering an excess mole of aqueous Mn(II) to be taken up by accompanying diagenetic mineral phases other than carbonates. An added prerequisite to the above is that sequential reduction of the primary metal oxyhydroxides, namely DMR followed by DIR, would have been mediated by the same consortium of metal-reducing bacteria. Combinations of DMR succeeded by DIR would thus be expected to generate carbonates with Fe/Mn ratios across space reflecting largely the variations in absolute and relative abundance of the two metals in the precursor sediment. However, the fact that both DMR and DIR reactions produce excess reduced metal compared to CO_2, in conjunction with the thermodynamic precedence of DMR over DIR (*e.g.,* Fröelich et al., 1979; Myers and Nealson, 1988; Nealson and Myers, 1990), would favour formation of manganiferous siderite with highest potential for near-quantitative uptake of Mn(II) as opposed to Fe(II). This would expectedly translate into strongly antithetic relationships between carbonate-hosted Mn *versus* Fe on a variety of scales, in response to variability in the primary fluxes of Mn oxides to the original sediments.

The key difference between DMR and DIR would lie in the higher oxidative capacity of MnO_2 compared to $Fe(OH)_3$, *i.e.*, two *versus* four moles of each respectively required to oxidise one mole of organic carbon. It should be stressed that the above principles would also apply if the primary budget of manganese in the precursor sediment involved Mn(III) oxyhydroxides (such as MnOOH) as well, with only consequence the relatively lower oxidising capacity of Mn(III) as compared to Mn(IV). Nevertheless, DMR does not rule out the potential of inherent availability of aqueous Mn(II) in pore-fluids prior to the onset of microbial diagenesis, and thus the possibility of contributions of pore-fluid Mn(II) to diagenetic carbonate growth. The strong bias of manganese partitioning into carbonate minerals compared to silicates and oxides, also introduces one key constraint in terms of chemical mass balance during diagenetic mineral formation *sensu lato*: namely, that carbonate minerals cannot readily form from (fluid-assisted) replacement of oxide or silicate minerals and *vice versa*, unless diagenetic mineral transformations were always open with respect to manganese and carbon.

1.3. Impact of manganese on the interpretation of stable isotope systematics in IF

Diagenetic uptake of re-mineralised organic matter (assumed average $\delta^{13}C \sim -25‰$) into IF carbonates, is supported in principle by their globally negative $\delta^{13}C$ values (generally ranging between -13 and $-5‰$; Baur et al., 1985; Beukes and Klein, 1990; Kaufman et al., 1990; Tsikos et al., 2003) compared to that of typical marine DIC ($\sim 0‰$). The processes of DIR and DMR intrinsically and proportionally link the production of Fe(II) and Mn(II) in the primary sediment with that of organic carbon recycling and delivery of carbonate alkalinity (Johnson et al., 2003, 2005; Heimann et al., 2010; Posth et al., 2013). It follows that Fe-Mn carbonate formation would have depended almost entirely on localised carbonate alkalinity maxima driven by DIR and DMR reactions within the sediment pile; other, abiotic pathways for Mn (IV,III) reduction to Mn(II), such as through reaction with water-column or pore-fluid Fe(II), would have to be eliminated from consideration. For the same reasons, diagenetic carbonate formation

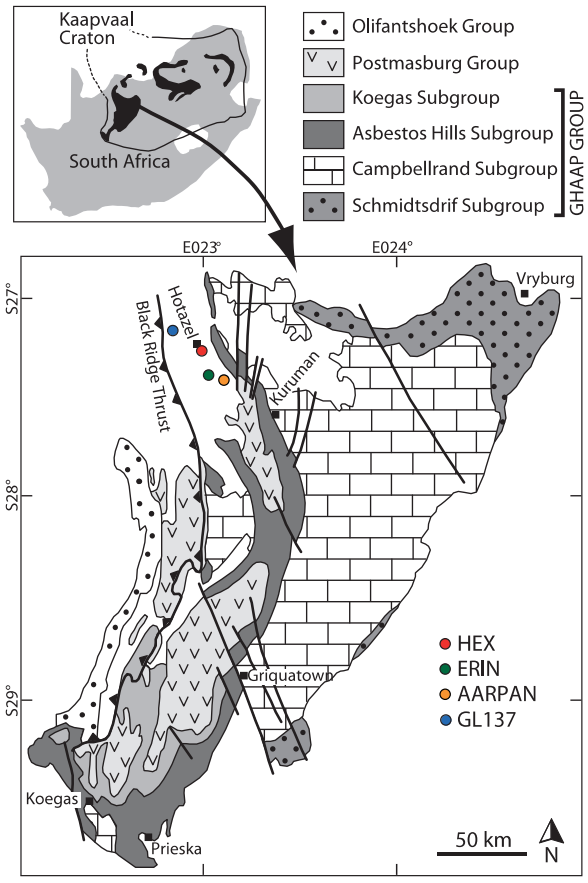

Fig. 2. Geological map and regional stratigraphy of the Transvaal Supergroup in the Northern Cape Province of South Africa, including localities of all four drillcores used in this study (ERIN, AARPAN and HEX for the Griquatown and Kuruman IF; GL137 for the Hotazel IF).

through other pathways would also have to be essentially excluded. The modal abundance and variability of Fe(+Mn) carbonate minerals in IF would then be a direct function of the primary fluxes of organic carbon to the sediment as the main electron donor.

In light of the above, partitioning of non-redox sensitive alkali earth elements (Ca and Mg, and less so Sr and Ba) into diagenetic carbonate minerals, could only be explained by replacement reactions involving Fe/Mn carbonates along with Ca/Mg-bearing counterparts that precipitated – inorganically or biogenically – out of seawater (Heimann et al., 2010). Such diagenetic reactions would lead to mixing of seawater-derived DIC with CO_2 produced microbially within the sediment *via* DIR and DMR, and hence to the intermediate $\delta^{13}C$ values between those of end-member seawater DIC and bulk organic carbon (~0 and ~−25‰ respectively). The $\delta^{13}C$ values of IF carbonates would, therefore, be expected to vary widely in accordance with their compositional characteristics: for example, pure Fe/Mn end-members predicted to have formed entirely through DIR and DMR reactions would be expected to have the lowest C isotope ratio, whereas Ca- and Mg-rich carbonate minerals would record higher $\delta^{13}C$ values (see, for example, Johnson et al., 2003; Heimann et al., 2010).

Shuttling of redox-sensitive trace metals (*e.g.,* Mo, Co, Tl) *via* primary Mn(IV) oxide deposition in IF (*e.g.,* Swanner et al., 2014; Kurzweil et al., 2016; Ostrander et al., 2019), is also a key pre-condition for the interpretation of related non-traditional stable isotope systematics. Popular interpretations of trace metal isotope ratios (mainly of Mo) suggest that primary Mn(II) oxidation to Mn(IV) from episodic oxygen whiffs and adsorption of redox-sensitive metals onto Mn(IV) oxides, would have exerted the main control on corresponding isotopic fractionation effects (Planavsky et al., 2014; Kurzweil et al., 2016). Quantitative sequestration of manganese – and of the trace elements putatively associated with it – into diagenetic minerals is therefore an integral requirement for primary signal preservation and thus reliable paleo-redox interpretations. By definition, quantitative precipitation of redox-sensitive metals precludes any open-system escape from the sediment pile during diagenetic re-mobilisation. Prevalence of oxic conditions across the entire water column (Ostrander et al., 2019) would thus have been essential for rapid re-oxidation and re-deposition of any outward-diffusing, soluble ionic species of these metals from the sediments into benthic seawater.

Recent speciation results from the Paleoproterozoic IF of South Africa (Kuruman, Griquatown; Oonk et al., 2017) have shown that, in stark contrast to manganese, practically all other redox-sensitive trace metals in IF occur in very low concentrations (*e.g.,* average Mo = 0.84 ± 0.47 ppm) and show variable partitioning into all major mineral groups (silicates, oxides and carbonates). A consequent assumption for the interpretation of redox processes based on these trace metals is that they quantitatively sequestered into a variety of secondary mineral phases during diagenesis, and not exclusively in the carbonate minerals which simultaneously serve as the overwhelming hosts of manganese. An additional assumption central to confident interpretations of trace metal isotope systematics in IF, is that their entire budget in the rocks is associated only with primary Mn(IV) precipitation and with no other pathway whatsoever. This assumption becomes an imperative in view not only of the variable speciation for most of these metals but also of their vanishingly low bulk-rock abundances as recorded in IF (Oonk et al., 2017; Thibon et al., 2019).

2. Rationale

In this paper, we examine in detail, assess and interpret the abundance of manganese, its mineral partitioning, overall distribution and possible primary and secondary depositional controls, in one of the best developed IF sequences of the Paleoproterozoic sedimentary record, namely the Transvaal Supergroup in the Northern Cape Province and associated (stratigraphically from older to younger) Kuruman, Griquatown and Hotazel IF (Beukes and Klein, 1990; Oonk et al., 2017; Figs. 1, 2). Recent results from particularly the first two IF have provided comprehensive geochemical information on bulk-rock and mineral fraction-specific levels, using optimised sequential extraction procedures (Oonk et al., 2017, 2018). These results revealed appreciable variability with respect to manganese abundance in the rocks, with highest values consistently recorded in the carbonate fraction of approximately the upper half (ca. 120 m) of the total stratigraphic thickness of the Griquatown IF from several drillcore intersections (Figs. 1, 2). Correspondingly high bulk carbonate modal abundances would also rank the Griquatown IF as possibly one of the most carbonate-rich IF on record.

Recent research (Warke et al., 2020a) has highlighted the possibility that the GOE would have preceded the earliest snowball Earth event postulated to have taken place at approximately 2.4 Ga, as exemplified by the Huronian glacial deposits in N. America and age-equivalent formations elsewhere in the world (Hoffman, 2013). In the study area (Figs. 1A, 2), such glacial deposits are represented by a diamictite layer known as the Makganyene Formation of the basal Postmasburg Group, which rests directly on the Griquatown IF through an apparently conformable contact (Fig. 1B). Recent radiometric age constraints from the Ongeluk volcanic rocks overlying the Makganyene Formation (Gumsley et al., 2017), point to a minimum age for the Griquatown strata at 2.43 Ga (Fig. 1A). The study of Warke et al. (2020a) has therefore added increased significance to this age relationship and its implications, as it effectively places the GOE in broad synchronicity with the deposition of the Griquatown IF. Consequently, our emphasis was directed mainly on the Griquatown rocks with respect to their carbonate mineralogy and possible controls on their carbonate-hosted manganese

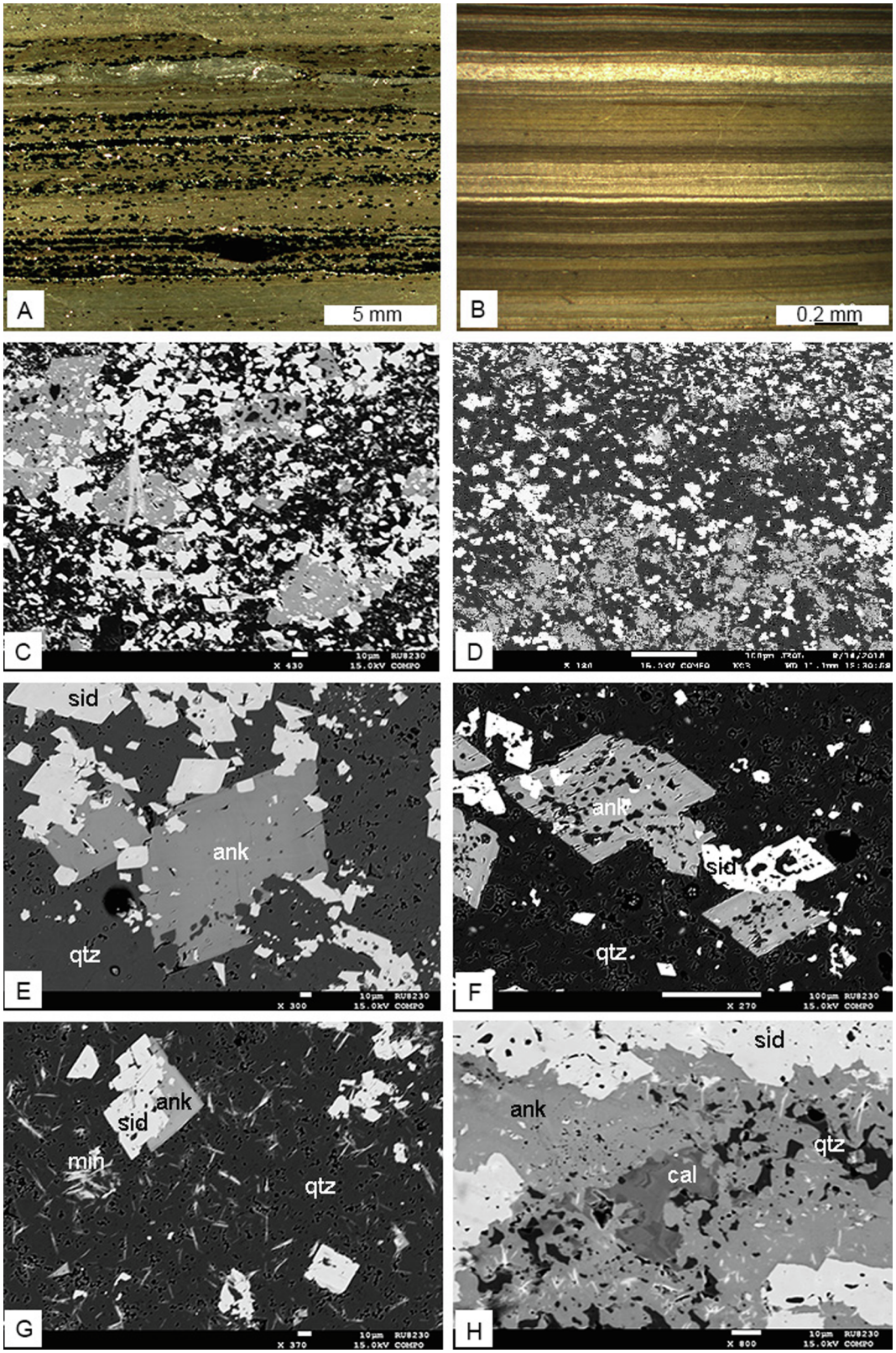

Fig. 3. Thin-section and back-scattered electron (BSE) images of carbonate minerals from selected samples of this study. Image A illustrates microbanded texture as exemplified in the Griquatown IF, whereas image B shows classic microbanding that typifies the Kuruman IF (samples E70 and E1 respectively). Images C and D (samples E70 and HOT respectively) illustrate first-order textural attributes and distribution of coexisting ankerite and siderite; in both instances, relatively brighter and generally smaller carbonate rhombohedra represent siderite (due to its higher Fe content compared to ankerite). Images E, F and G (samples E66, E60 and E59 respectively) display fine-scale textural associations between ankerite and siderite, namely: clusters and disseminations of fine euhedral siderite around larger ankerite rhombohedra (E); rhombohedra of ankerite and siderite with abundant quartz inclusions in a chert matrix (F); and apparent equilibrium intergrowth of ankerite and siderite in a quartz-minnesotaite matrix (G). Image H (sample E1) illustrates relic high-Mg calcite replaced by subhedral aggregates of ankerite, with siderite dominating in the outer margins.

content. For comparative purposes, we have also included one sample from the Kuruman IF, as well as a single sample from the younger Hotazel IF, both of whom contain – on average – relatively lower modal carbonate and corresponding manganese contents than those recorded in the Griquatown IF.

It should be noted that the Griquatown IF is also known to contain a substantial proportion of granular facies assemblages on mm- to cm-scales, which have been interpreted previously as products of episodic deposition in a high-energy paleo-depositional environment above wave-base (Beukes and Klein, 1990). Due to the possibility of post-depositional re-working of primary IF sediment in the Griquatown paleoenvironment leading to detrital-style accumulations of granules, we have chosen to omit from this study the inclusion of any results from the granular subfacies itself. We have instead concentrated our current approach on abundant, fine-grained, carbonate-bearing banded assemblages in the Griquatown samples, which also typify classic microbanded facies such as those that characterise the Kuruman and Hotazel IF (Figs. 3A-B).

3. Materials and methods

We selected 16 samples containing variable bulk MnO contents from four drillcore intersections (Fig. 2); three of these captured the Griquatown and upper Kuruman IF (ERIN, AARPAN, HEX) whereas drillcore GL137 intersected the Hotazel IF and interbedded Mn-rich layers. A total of 14 samples represent the entire stratigraphic extent of the Griquatown IF (Fig. 1), one sample (E1) comes from the topmost Kuruman IF, and one sample (HOT) from the upper part of the Hotazel IF. Our sample selection was informed by a combination of standard petrographic observations and corresponding bulk geochemical results, particularly variations in measured MnO in bulk rock and the carbonate-specific fraction thereof as reported previously for the Kuruman and Griquatown IF (Oonk, 2017; Fig. 1A). Our petrographic work involved examination of polished thin sections under the polarising microscope. Petrography was accompanied by applications of scanning electron microscopy (SEM) coupled with qualitative microanalyses, using an attached energy-dispersive spectrometer (EDS) at Rhodes University. Over 900 quantitative mineral-chemical analyses from a corresponding number of random carbonate grains – known to contain the bulk of manganese in these rocks – were carried out using an electron microprobe (EPMA) at Rhodes University.

A total of 16 polished thin sections were carbon-coated under vacuum to 25 nm (± 5) thickness. The coated sections were examined and analysed using a Tescan VEGA Scanning Electron Microscope (SEM) operated at 20 kV. Qualitative elemental analysis and compositional element maps were obtained using an Oxford INCA PENTA FET X3 Energy-Dispersive Spectrometer (EDS) attached to the SEM. Quantitative mineral-chemical analyses and X-ray maps for carbonate minerals were produced using four wavelength dispersive spectrometers on a JEOL JXA-8230 electron probe micro-analyzer. The beam was generated by a Tungsten cathode, and excited with 15 kV accelerating potentials at beam currents of 20 nA (quantitative) and 60 nA (mapping). Due to the very fine size of carbonate grains, a focused beam was used, following a few representative control analyses with a broader beam to characterize the magnitude of potential analytical differences. Elements were measured on K-alpha peaks except for Sr and Ba which were measured on L-alpha peaks. Counting times on peak were 10 s, and 10 s total on background. Commercial “SPI” standards were used for intensity calibration: the standards were Pyrope (Si, Ca, Fe), Dolomite (Mg), Rhodonite (Mn), Strontium Titanate (Sr), and Barite (Ba). Data were collected with JEOL software (PC EPMA 1.9.2.0) and its ZAF matrix algorithm (Heinrich/Duncumb-Reed with FFAST-2005 MACs) was applied to correct for differential matrix effects. Oxygen was calculated by stoichiometry. Theoretical calculations of contained CO_2 were also performed against the elemental oxide determinations, and the closeness of the ensuing total sums to the value of 100 was used as measure of analytical quality. All raw analytical data are archived in the Supplementary Information Data File.

Petrographic and micro-analytical results have been complemented by carbonate-carbon isotope analyses of two samples, namely ARP1 and E60, in which the co-existence of three distinct carbonate mineral phases (*i.e.,* calcite, ankerite and siderite) is documented. All $\delta^{13}C$ values, *i.e.,* bulk-rock and mineral-specific, are reported relative to V-PDB, whereas $\delta^{18}O$ values (where applicable) are quoted relative to V-SMOW. A single bulk-rock $\delta^{13}C$ analysis for each of the above two samples was first obtained at the stable isotope laboratory of SUERC, East Kilbride, Scotland. Isotope ratio measurements were made on an Analytical Precision AP2003 mass spectrometer equipped with a separate acid injector system, after reaction with pure H_3PO_4 under a He atmosphere at 70 °C. Samples were acidified for a minimum of 7 days in both cases to ensure full digestion of siderite. Mean analytical reproducibility based on replicates of the SUERC laboratory standard MAB-2 (Carrara Marble) was around ± 0.2‰ for both carbon and oxygen. Moreover, for the most carbonate- and Mn-rich sample of the two (*i.e.,* ARP1), sequential $\delta^{13}C$ and $\delta^{18}O$ values were obtained in quadruplicate, following the protocol of Al-Aasm et al. (1990). Specifically, four sub-samples of sample ARP1 were pulverised separately and approximately 30 mg of each were reacted in pure H_3PO_4 sequentially at 25 °C, 50 °C (in water bath) and 100 °C (in paraffin bath) for 3, 12 and 1 h respectively, at the stable isotope laboratory of the University of Cape Town. In all cases the reaction had gone to completion judging by the lack of effervescing CO_2. The above methodology permitted the extraction of average $\delta^{13}C$ values (in quadruplicate), that are specific to the three respectively reactive carbonate fractions of sample ARP1 under the aforementioned conditions, namely calcite (25 °C), ankerite (50 °C) and siderite (100 °C). Because all of the C in the sample is transformed to CO_2, the magnitude of the acid fractionation factor is not important, nor is the exact temperature of the reaction. The in-house calcite standard NM ($\delta^{13}C$ = 1.57‰, $\delta^{18}O$ = 25.10‰) was analysed in duplicate with the samples and extracted at 25 °C, and the data used to convert raw data to the PDB and SMOW scales.

4. Results

Ankerite and siderite are the omnipresent carbonate minerals in the examined IF samples – Ca/Mg-rich, Fe/Mn-poor equivalents (*e.g.,* calcite) are, by contrast, uncommon but nevertheless also occasionally present. Ankerite is usually the coarser-grained and, in most instances, the modally dominant carbonate, as compared to siderite which is generally finer-grained and less abundant (Figs. 3C–F). Relative modal abundances of the two carbonates can, however, vary from ankerite- to siderite-dominated domains, on scales as small as a single sub-mm band (Figs. 3C and D). Individual grains exhibit common rhombohedral terminations resulting in the characteristically subhedral to euhedral habit of carbonate minerals (Figs. 3C–G). Such grains may be entirely made up of carbonate, but most frequently contain micro-inclusions of quartz (Fig. 3F) and much less so of other minerals (*e.g.,* magnetite). Textural attributes between co-existing ankerite and siderite can be complex and intricate, pointing to possibly simultaneous equilibrium crystallisation over large part of their formation history (Figs. 3E–G). Textures that could be interpreted as strongly indicative of successive paragenetic growth of the two carbonates (such as siderite overgrowth rims surrounding ankerite cores and *vice versa*), were not observed in our samples. In general, however, small rhombohedral siderite populations appear to be concentrated on and around the margins of larger ankerite rhombohedra, suggesting that the two carbonates may have followed, at least partly, a sequential pattern of crystallisation.

In terms of chemical composition, ankerite grains are effectively invariant in CaO content across the entire sample set studied, at average values from 27.1 ± 0.4 wt% (sample ARP20) to 29.0 ± 0.8 wt% (sample E59). Average ankerite FeO contents show comparatively larger variability, with minima registered in sample HOT at

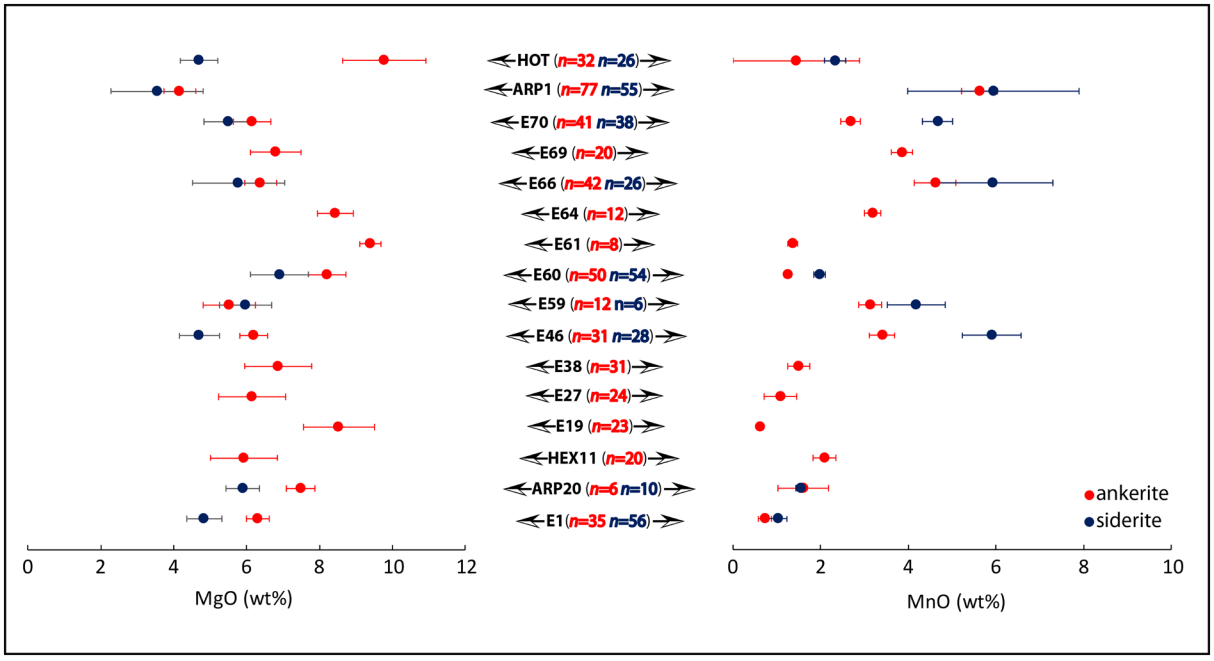

Fig. 4. Diagrams illustrating mean MgO and MnO EPMA data and error bars for ankerite and siderite grains from thin sections of all individual IF samples selected for this study. Results are arranged in broad stratigraphic order with lowermost sample E1 representing the older, Kuruman IF; uppermost sample HOT representing the younger, Hotazel IF; and all remaining samples representing the Griquatown IF.

15.5 ± 1.6 wt%, whereas maximum FeO is recorded in sample E27 at an average of 21.5 ± 1.5 wt%. Average ankerite MgO and MnO contents are likewise variable from sample to sample: maximum MnO content is recorded in ankerite from sample ARP1 at an average of 5.6 ± 0.4 wt%, whereas sample E19 registers minimum average ankerite MnO content at 0.6 ± 0.1 wt%. Similarly, average ankerite MgO content ranges from 4.2 ± 0.4 wt% (sample ARP1) to 9.8 ± 1.1 wt% (sample HOT). With respect to siderite data, average FeO contents vary narrowly from 45.3 ± 2.1 wt% (sample E66) to 53.3 ± 0.7 wt% (sample E1). Average siderite MgO content ranges from a minimum of 3.6 ± 1.3 wt% (sample ARP1) to a maximum of 6.9 ± 0.8 wt% (sample E60), whereas average MnO content ranges from as high as 5.9 ± 2.0 wt% (sample ARP1) to as low as 1.0 ± 0.2 wt% (sample E1). Siderite CaO contents are generally very low, with maxima registered only in sample E59 at an average of 2.3 ± 2.4 wt%.

Arguably the key common attribute of siderite and ankerite in terms of both MnO and MgO contents, is that both species record narrowly ranging values in each sample and thus very low standard deviations from the average. This is summarily illustrated in the two diagrams of Fig. 4. An additional feature of interest in terms of subsequent considerations and interpretations, is that at least in the few instances reported here where ankerite and siderite coexist on small scales, both carbonates show very closely comparable average MnO content, with siderite recording slightly higher concentrations at slightly higher variance (Fig. 4). The same can also be argued for average MgO contents which are very similar for both carbonates, yet with ankerite taking up marginally higher amounts of Mg than coexisting siderite (Fig. 4). These aspects will be revisited in the sections that follow.

An observation of potentially high interest in the context of this study is the detection of apparent remnants of a Fe/Mn-bearing, Mg/Ca-rich carbonate phase documented to variable extents in most of our samples, particularly in the more manganese- and carbonate-rich uppermost part of the Griquatown IF. This carbonate displays strong textural evidence for later replacement processes, which manifest through the development – successively from the grain margins outwards – of subhedral ankerite and siderite that appear to effectively consume the (earlier) carbonate grains (Fig. 3H). The degree of replacement varies from thin rims of micro-crystalline ankerite (+siderite) surrounding largely preserved masses of relic carbonate, to ankerite(+siderite) micro-aggregates containing small irregularly shaped inclusions of apparently un-replaced carbonate (Fig. 3H).

Backscattered electron (BSE) imaging coupled with EPMA compositional maps (Figs. 5, 6) and a large number of spot analyses (Figs. 7, 8) have revealed substantial compositional variability in the interpreted early carbonate phase. This applies especially with regard to MnO (9.0 ± 2.6 wt% for sample ARP1; 2.5 ± 0.7 wt% for sample E60) and CaO, which show a statistically strong anti-correlation in both samples, pointing to a systematic decoupling in the partitioning of Mn and Ca in the carbonate structure (Figs. 7, 8). The latter relationship, in combination with high yet largely invariant MgO contents (10.5 ± 1.0 wt% for ARP1; 15.7 ± 0.3 wt% for E60), collectively suggest that this specific carbonate mineral most likely represents a type of high-Mg, Fe/Mn-bearing calcite; we will therefore refer to this species hereon simply by the acronym “HMC” (High-Magnesium Calcite).

The variable compositional attributes of HMC contrast sharply with the very low variance in co-existing ankerite and siderite, as illustrated in Figs. 7 and 8. Nevertheless, both samples ARP1 and E60 show close correspondence in their average MgO and MnO concentrations of both ankerite and siderite when compared to those of the enclosed HMC. This relationship signifies a likely direct conservative control of HMC concentrations in Mn and Mg over those recorded in the ankerite and siderite that appear to replace it. The average FeO/MnO ratio of HMC, however, is close to the value of 1 in sample ARP1 and approximately 2 in sample E60, and therefore much lower than the corresponding ratios in coexisting ankerite and siderite. This leads to the requirement for substantial Fe(II) addition during HMC replacement reactions.

Bulk-rock $\delta^{13}C$ data for samples ARP1 and E60 containing HMC, are −6.4‰ and −9.5‰ respectively. Sequential analyses of sample ARP1 run 4 times gave $\delta^{13}C$ and $\delta\ ^{18}O$ values of −6.7 (± 0.2 2σ) and 17.6 (± 0.8 2σ) at 25 °C, −6.0 (± 0.2 2σ) and 19.7 (± 0.6 2σ) at 50 °C, and −6.2 (± 0.1 2σ) and 18.9 (± 0.7 2σ) at 100 °C. The average yields were 11.4 wt% at 25 °C, 21.8 wt% at 50 °C, and 39.6 wt% at 100 °C.

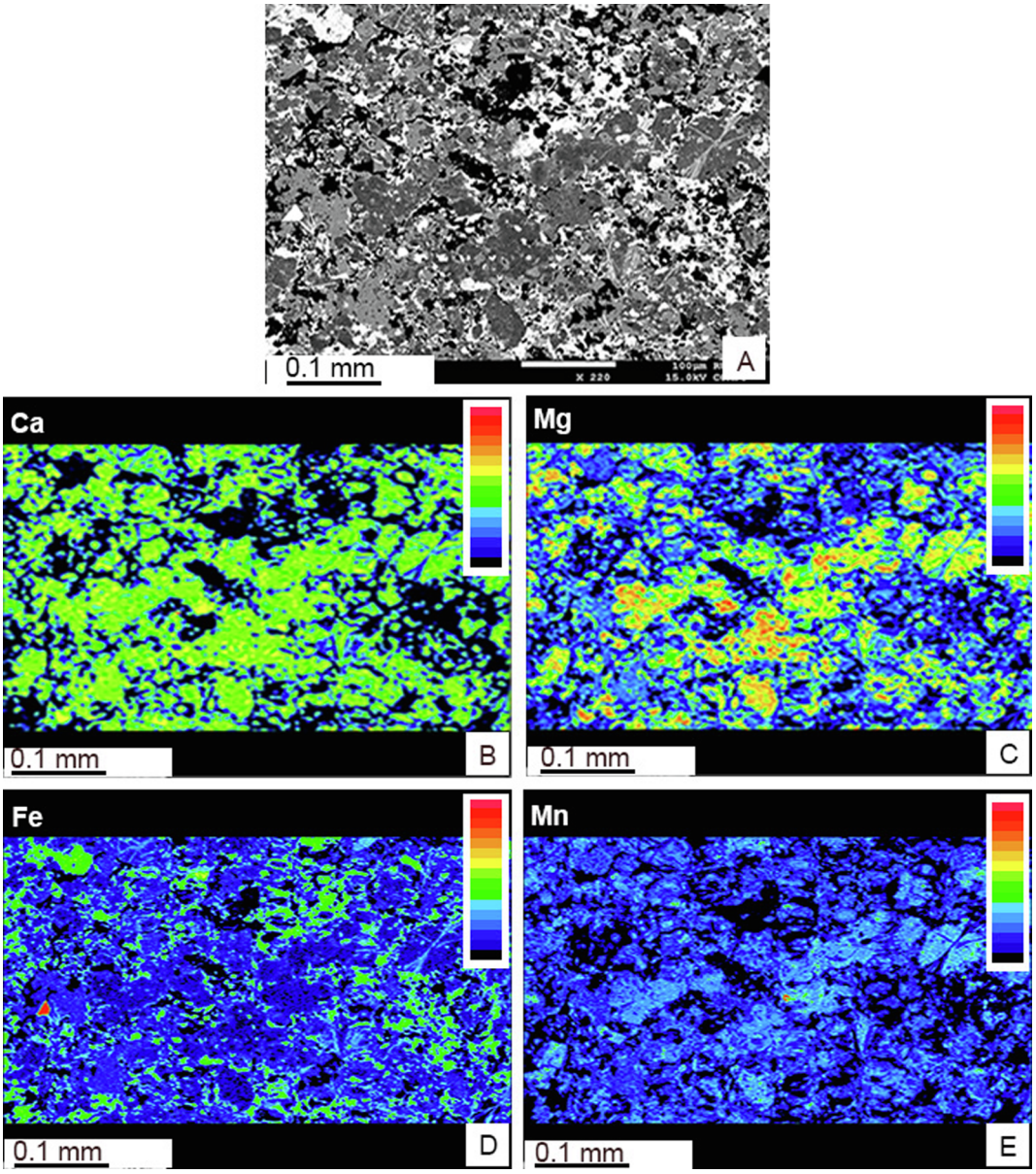

Fig. 5. Back-scattered electron (BSE) image (A) and corresponding compositional maps for Ca (B), Mg (C), Fe (D) and Mn (E), for sample ARP1. Note the patchy development of relatively high-Mg, low-Fe and high-Mn domains which correspond to preserved relics of HMC. Surrounding matrix is dominated by ankerite, quartz, lesser siderite, magnetite and minor minnesotaite.

5. Discussion

5.1. Manganese in IF in the context of dissimilatory Fe-Mn reduction during microbial diagenesis

The foregoing observations and results call for a possible re-assessment of established carbonate-forming pathways in IF, modes of manganese precipitation, and their collective implications. The starting point of choice in this discussion is the strikingly homogeneous composition of iron carbonate minerals on scales of a single thin-section and smaller. A hallmark of diagenetic models that place biologically-mediated Fe and Mn reduction (DIR and DMR) in IF at the centre of carbonate mineral formation, is that such processes are expected to result in the development of compositional and isotopic heterogeneities on fine scales, in response to small-scale variability in the mineralogy and chemistry of the primary precipitates (*e.g.,* Baur et al., 1985; Heimann et al., 2010). As succinctly discussed in the introductory sections of this paper, the operation of DIR and DMR relies fully and directly on the dominance of high-valence Fe- and Mn-oxyhydroxide precursors along with organic matter. Therefore, ankerite and siderite growth with essentially invariant compositions with respect to carbonate-forming cationic species (Ca, Fe, Mn and Mg), would require the operation of some sort of fluid-assisted homogenisation mechanism against chemically heterogeneous precursor material. This could have taken place through reductive dissolution of precursor metal oxide phases; chemical homogenisation (mixing) and, possibly, spatially limited re-mobilisation in pore fluids; and quantitative re-precipitation as neomorphic Fe/Mn-rich carbonates – either *in situ* or at suitable nucleation sites – in an essentially closed system. As mentioned earlier, closed system, quantitative precipitation is an essential requirement in order to preserve the utility and integrity of trace element chemical and isotopic signals (such as Mo isotopes) that would have accompanied the postulated Fe(III) and Mn(IV) oxyhydroxide precursors.

The evident dominance of ankerite in the examined IF samples and its widespread occurrence in other IF worldwide (*e.g.,* Klein and Gole, 1981; Baur et al., 1985; Beukes and Klein, 1990; Kaufman et al., 1990;

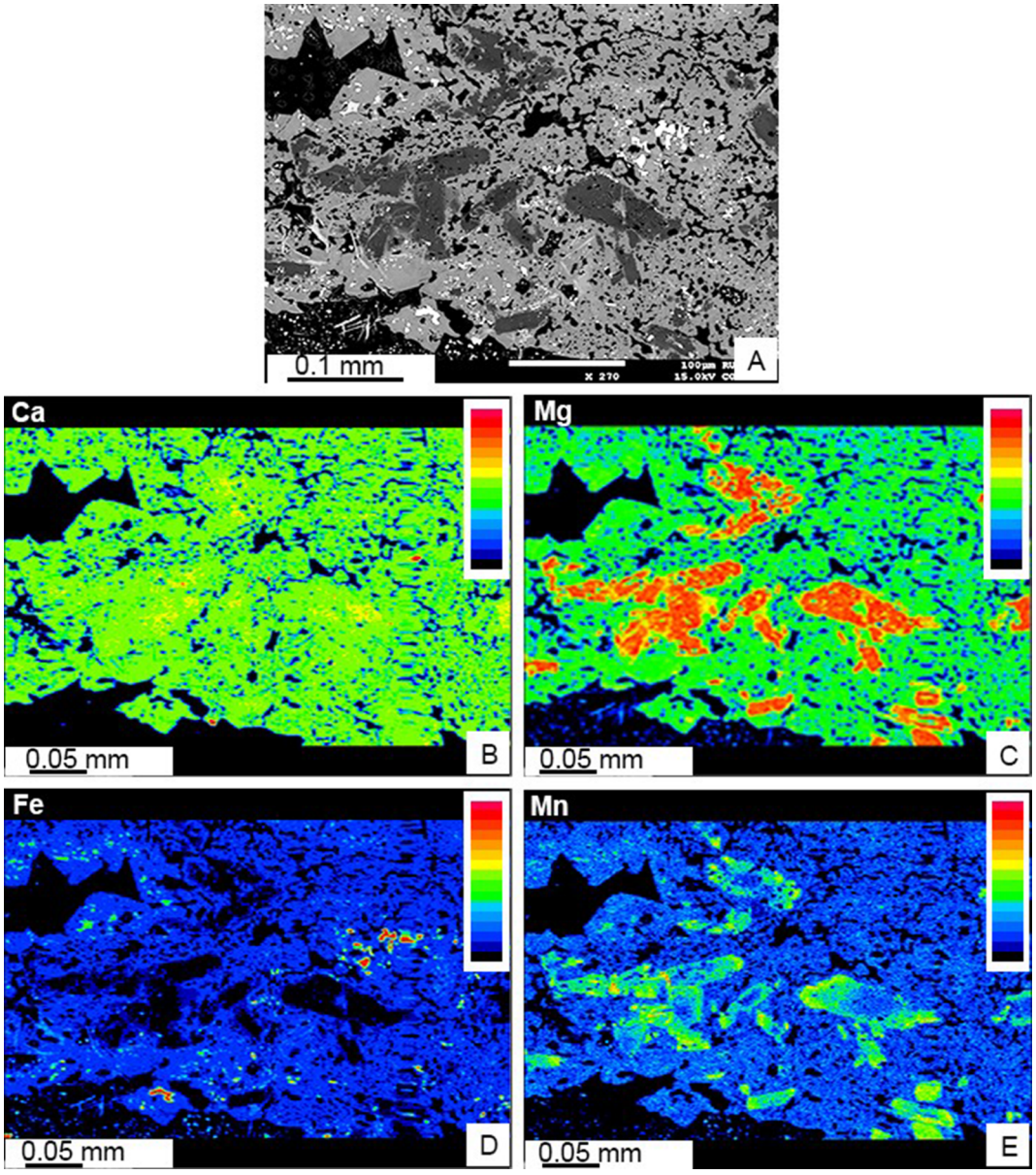

Fig. 6. Back-scattered electron (BSE) image (A) and corresponding compositional maps for Ca (B), Mg (C), Fe (D) and Mn (E), for sample E60. Note the patchy development of relatively high-Mg, low-Fe and high-Mn domains which correspond to preserved relics of HMC. Surrounding matrix is dominated by ankerite, quartz, lesser magnetite and minor siderite and minnesotaite.

Tsikos and Moore, 1997; Haugaard et al., 2016), poses an obvious question concerning the source of Ca, Mg and DIC leading to ankerite saturation and crystallisation. As discussed earlier, carbonate-forming reactions related to DIR and DMR would predict formation of pure end-member Fe- and Mn-carbonate minerals, as this has also been shown experimentally with respect to at least siderite (Posth et al., 2013). Therefore, ankerite and siderite formation with compositions like those reported in this paper, require inputs of Ca, Mg and DIC that are independent of DIR and DMR. Published speciation results of the carbonate fraction across the Griquatown and Kuruman IF (Oonk et al., 2017) have revealed an average carbonate-specific (CaO + MgO)/(FeO + MnO) ratio of 0.68, which implicates large modal $(Ca,Mg)CO_3$ contributions to the initial sediment (*ca.* 40% of the bulk carbonate on average). These could have been attained either from pore-fluid supply of Ca(II), Mg(II) and DIC during diagenetic carbonate growth, and/or from primary carbonate precipitation out of seawater, possibly in the form of Mg-bearing calcite. The relative balance of marine-sourced *versus* DIR/DMR-linked carbonate species in the primary sediment, would thus dictate the average chemical and isotopic compositions of the ensuing ankerite and siderite populations.

The above considerations raise several questions with respect to carbonate formation in IF: for example, was Ca/Mg carbonate formation out of seawater possible during deposition of IF? The appreciable Ca and Mg abundances recorded in ankerite and siderite of this study, suggest that it must have been so. Was marine carbonate precipitation an ongoing or episodic process in terms of primary rates and fluxes of carbonate supply to the precursor sediments? Highly variable ratios of carbonate-hosted (CaO + MgO)/(FeO + MnO) from sample to sample would suggest correspondingly variable rates of primary carbonate deposition, and/or variability in carbonate preservation during open-system diagenesis. The latter, however, cannot be considered further in this discussion as it is in conflict with the requirement for closed-system conservation of the primary manganese fluxes to the sediments and their associated chemical and isotopic signatures. Finally, uncertainties also exist concerning the precise composition of seawater carbonate precipitates, namely whether they would have been in the form of pure

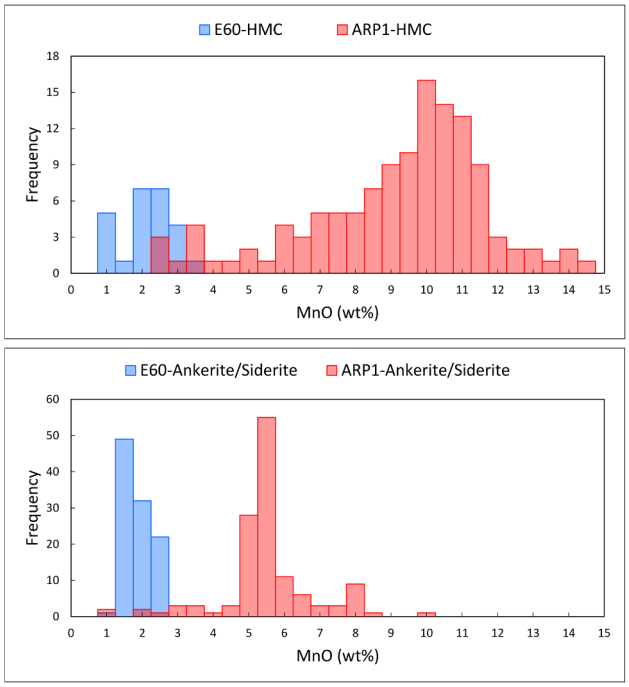

Fig. 7. Histograms illustrating variability in MnO content of HMC from samples ARP1 and E60, by comparison to corresponding data for co-existing ankerite and siderite. Note the different vertical scale between the two histograms.

$CaCO_3$, HMC/aragonite, or a carbonate phase containing at least some Fe(II) and Mn(II) in its structure. The latter possibility would have important implications, as uptake of Mn(II) into primary carbonate precipitates would mean that not all manganese present in IF would necessarily have to have derived from a high-valence oxyhydroxide precursor.

The documentation of apparently residual HMC in selected samples of this study sheds crucial new light on the origin of carbonate minerals in IF. Its presence, and especially its textural and interpreted paragenetic association with co-existing ankerite and siderite, represents to our knowledge one of the very few (if not the only to date) reports in literature of an apparent precursor carbonate mineral in IF acting as substrate for Fe(+Mn)-carbonate mineral formation. Reconciling the latter through classic models of DIR and DMR, represents an obvious challenge. In principle, formation of HMC is not consistent with redox reactions associated with DIR and DMR, given the generation of excess Fe(II) and Mn(II) per mole of organic carbon oxidized, and the widely reported inhibition of calcite formation in aqueous environments dominated by the presence of abundant Mn(II) and Fe(II) ions (*e.g.,* Dromgoole and Walter, 1990). Therefore, the only plausible way that the observed HMC would be compatible with DIR and DMR, is if it represents the intermediate member in a complex array of diagenetic reactions, which would have successively involved:

1. Primary deposition of organic matter and Fe/Mn oxyhydroxides, at Fe/Mn ratios (1–2) that were atypically low by comparison to corresponding whole-rock compositional ratios of IF;
2. Bacterially mediated diagenetic reactions following principles of DMR/DIR, that delivered Fe(II), Mn(II) and CO_2;
3. Formation of HMC *via* either:

a. quantitative (with respect to at least manganese) generation of diagenetic Fe-Mn carbonate which immediately reacted with primary, Fe/Mn-lean Mg calcite; or,

b. mixing of DIR/DMR-produced Fe(II), Mn(II) and CO_2 with abundant aqueous Ca(II), Mg(II) and DIC in the ambient pore-fluid, to drive saturation with respect to HMC;

4. Subsequent partial to complete replacement of HMC by neomorphic ankerite and siderite; this would have been largely conservative with respect to the chemical transfer of Ca, Mg and Mn, but would have required further major uptake of Fe(II) from pore-fluids.

In addition, the above sequence of processes would have been accompanied by quantitative sequestration into various minerals, of all redox-sensitive trace elements (*e.g.,* Mo, Tl, Co) and their stable isotope signatures that are interpreted to be linked to primary precipitation of Mn(IV) oxyhydroxides.

5.2. Manganese deposition through primary carbonate precipitation

An alternative and arguably more parsimonious interpretation of our new results, exploits the possibility that primary precipitation of carbonate minerals in IF may have been operative out of the oceanic water mass, in the form of Fe/Mn-bearing HMC. Such an interpretation is informed to a large degree, by recent studies aiming to address the universal lack of organic carbon preservation in IF, in conjunction with the low-$\delta^{13}C$ signature of the contained iron carbonate minerals (Dodd et al., 2019; Thompson et al., 2019). The study of Thompson et al. (2019), in particular, proposes that much of the organic matter generated through photoferrotrophy and/or oxygenic photosynthesis, would not have sequestered into precursor IF sediment in a congruent fashion to primary Fe oxyhydroxide precipitation. The resultant under-supply of organic matter to the initial IF sediment, would have resulted in quantitative organic remineralisation by the abundant Fe(III) oxyhydroxides, and would have also required the contribution of seawater carbonate precipitation out of an isotopically heavy DIC pool. The postulated "mixing" that would have resulted through these overlapping primary and diagenetic carbonate-forming pathways, would account for the generally intermediate carbon isotope composition of iron carbonate minerals in IF which, as indicated in earlier sections, has a typical range between −13 and −5‰.

Figure 9 presents a graphical depiction of the key elements of our alternative interpretation. Primary HMC formation would have taken place in the shallow oceanic environment under conditions of increased carbonate alkalinity. The atypically low Fe/Mn ratio recorded in the HMC compositions reported here (as low as < 1; see "Results" section earlier), would reflect water-column processes of relative aqueous Mn (II) enrichment contemporaneously with ongoing Fe(III) precipitation. Such Mn enrichment may have been essentially passive, for example through photoferrotrophic reactions excluding Mn(II) as a suitable electron donor. Alternatively, should Mn(II) oxidation have been transiently possible, we anticipate that its deposition as primary Mn oxyhydroxides would have been largely prevented through effective reduction of Mn(III) and/or Mn(IV) by abundant $Fe(II)_{aq}$ in the ambient anoxic water column. These processes would have resulted, either singly or in combination, in the development of a gradient of decreasing Fe/Mn ratio in shallow seawater, with minima recorded in the photic zone where biological Fe(II) oxidation was operative (Fig. 9)

Initial incorporation of Mn(II) and Fe(II) into the HMC at variable ratios (and of other divalent species at much lower abundances) would have been a function of the exact – but presently unconstrained – pathway of calcite formation (*e.g.,* inorganic saturation with respect to HMC, microbial calcification, etc.) in combination with the chemistry of the seawater parcel where primary carbonate nucleation occurred. Variability in the relative rates of metal (Fe, Mn) *versus* alkali earth (Ca, Mg) uptake through time, may therefore have been dependent – at least partly – upon temporally changing physico-chemical gradients with water depth. The same principles would also apply with respect to the low $\delta^{13}C$ value of primary HMC, which can be linked to processes of redox cycling – aerobically or anaerobically – of reduced C species in the water column (*e.g.,* organic matter and possibly also methane), and mixing of the isotopically light CO_2 produced with the long-term oceanic DIC reservoir of a $\delta^{13}C$ value at near-zero ‰ (Swanner et al.,

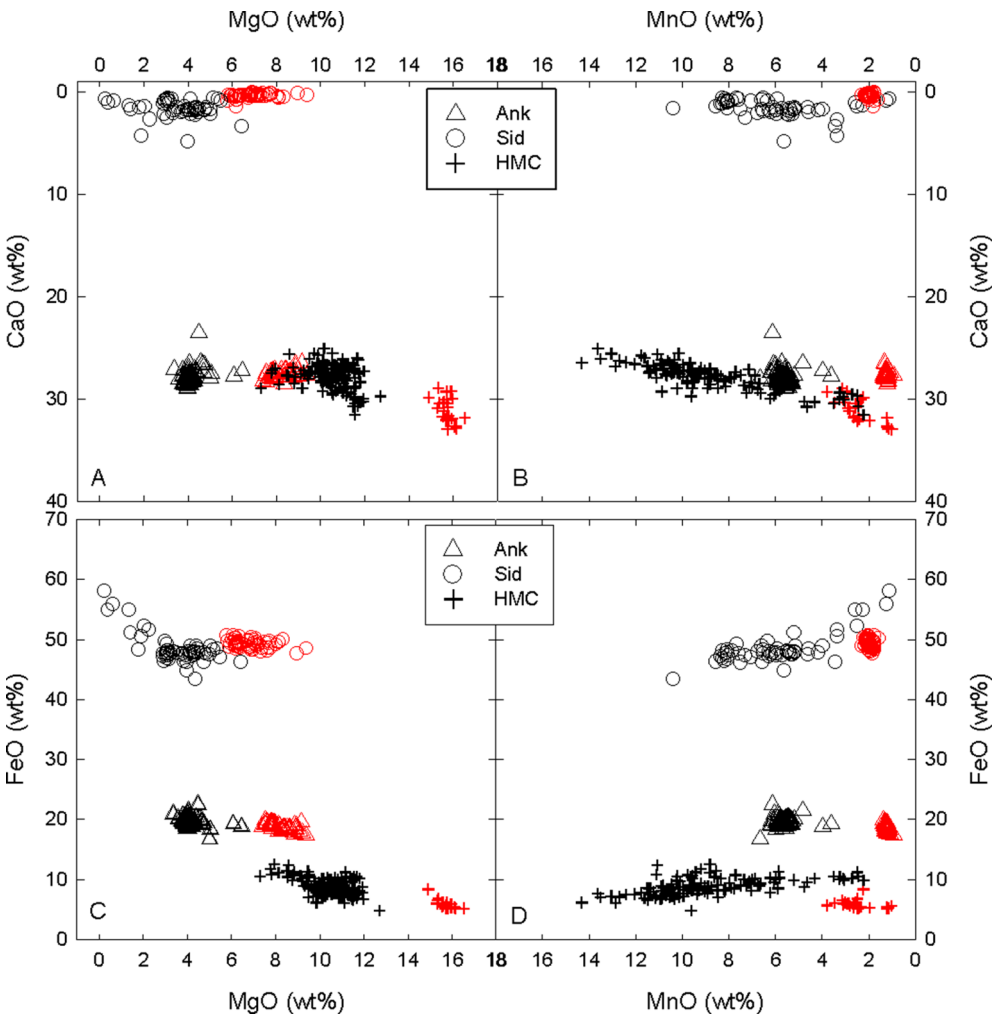

Fig. 8. Binary plots illustrating compositional relationships for co-existing HMC, ankerite and siderite for samples ARP1 (black symbols) and E60 (red symbols). Note the high variability and strong anti-correlation between CaO and MnO in HMC (plot B). (For interpretation of the references to colour in this figure legend, the reader is referred to the web version of this article.)

2018; Wittkop et al., 2020; see also Fig. 9). Crucially, the above interpretation implicates no primary Mn oxyhydroxides as effective carriers of redox-sensitive trace elements to the sediment, although Mn oxyhydroxide formation – whether transient or ongoing – may still have played an important role (along with Fe oxyhydroxides) in supplying additional electron acceptors to oxidative organic matter (and/or methane) recycling within the oceanic water column (Wittkop et al., 2020).

The primary marine carbonate precipitate would have been locally preserved as the observed Fe/Mn-bearing HMC. Partial to complete solid-state replacement and/or dissolution followed by rapid re-precipitation reactions at the expense of this early-formed carbonate in the presence of Fe(II)-rich pore-fluids, would have led to saturation and diagenetic formation of chemically homogeneous ankerite and siderite (Fig. 9). From a compositional point of view, this would have been attained essentially *via* Fe(II) addition only, derived from diagenetic pore-fluids whose composition was controlled by that of overlying ferruginous bottom waters. It is expected that the corresponding Fe/Mn ratio of such waters may have been at least as high as that of average crust (50/1), in general accordance with the high bulk-rock Fe/Mn ratio that characterises most IF (Klein, 2005). By contrast, the absolute and relative abundances of other carbonate-contained components (*i.e.,* Ca, Mg and Mn) would be accounted for largely through conservative redistribution and homogenisation from the precursor HMC compositions. Therefore, variability in the absolute abundances and relative ratios of Mn and Mg in ankerite and siderite from sample to sample, can be interpreted in each instance as being inherited directly from parent HMC. The extent of iron carbonate formation would have been dependent on the degree of CO_2 availability: *in situ* bulk replacement processes would utilise the HMC-bound CO_2 and may have involved additional DIC contained in pore-fluids, ultimately derived from the deep-water marine reservoir. The same would apply to processes of dissolution and mixing of primary HMC-sourced CO_2 with pore fluid DIC, resulting in transient maxima in carbonate alkalinity that were evidently conducive to ankerite and siderite saturation and subsequent crystallisation.

Our new carbonate-carbon isotope data provide strong additional support to our above interpretation. On the basis of earlier arguments presented in this paper regarding anticipated isotopic signals related to DIR and DMR pathways of carbonate formation, the two bulk $\delta^{13}C$ values appear to be at clear odds with such processes. Specifically, sample E60 containing the more impoverished HMC compositions in terms of combined iron and manganese content, has a bulk $\delta^{13}C$ value that is over 3‰ lower than the HMC from sample ARP1 which contains more than twice as much combined iron and manganese in its structure. The mineral-specific $\delta^{13}C$ data for sample ARP1 yield further clues against a DIR/DMR mode of formation, in that the ankerite and siderite $\delta^{13}C$ values are very similar to, and thus also apparently buffered by, the $\delta^{13}C$ composition of earlier HMC. Expected differences between dolomite (ankerite) and HMC, and between siderite and HMC $\delta^{13}C$

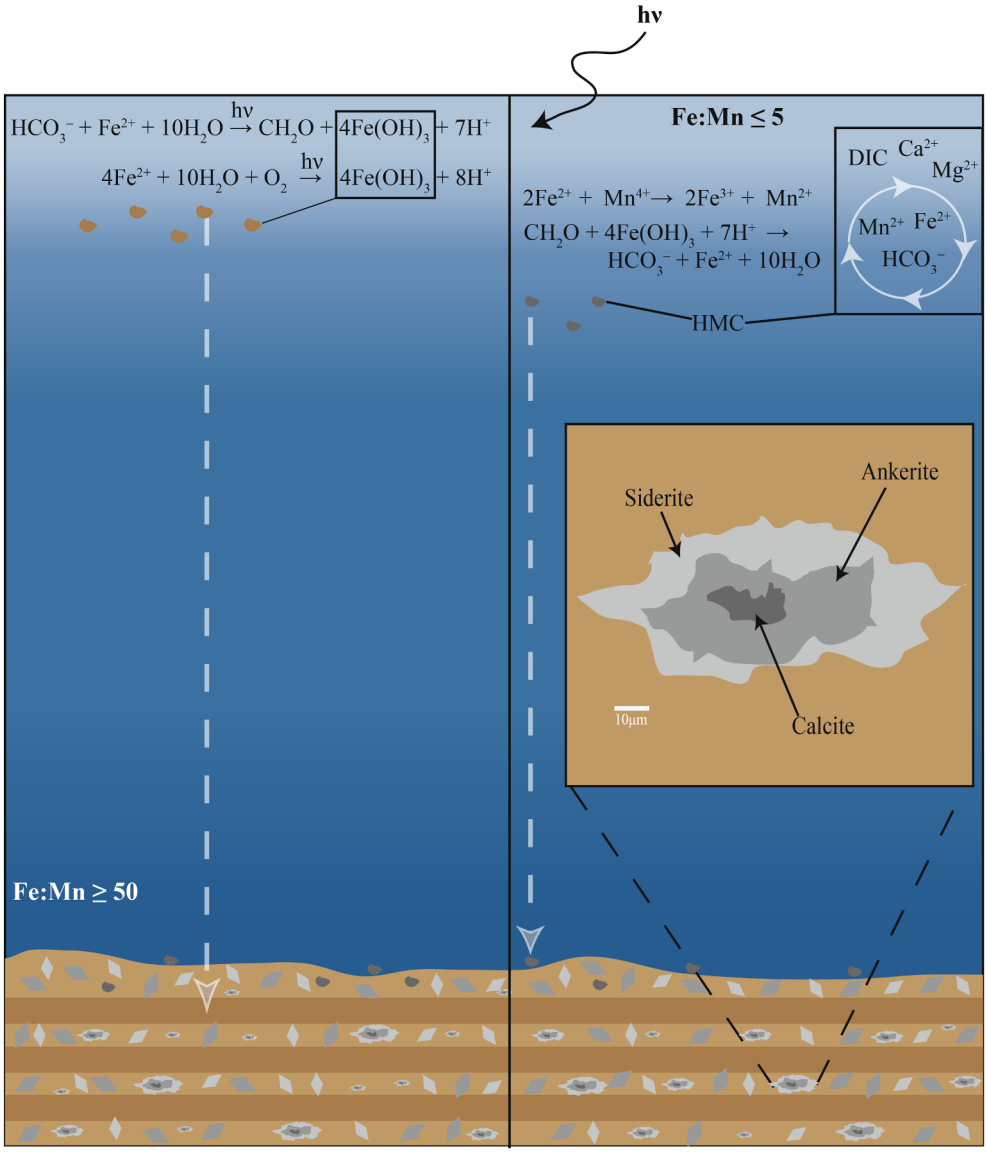

Fig. 9. Box model illustrating the essential elements of primary HMC precipitation during deposition of the Asbestos Hills IF, and its subsequent replacement by diagenetic ankerite and siderite. Unidirectional deposition of ferrihydrite through photoferrotrophy and/or oxidation of Fe(II) by photosynthetic O_2, including the corresponding basic reactions, are shown on the left-hand side of the diagram. The resultant ferrihydrite-rich layers would have given rise diagenetically to the commonly observed magnetite microbands in IF, as a result of reaction of ferrihydrite with pore-fluid Fe(II). The right-hand side of the diagram shows proposed pathways of primary HMC formation as a result of water-column redox cycling and shallow-water enrichments in Mn (II) and carbonate alkalinity. The two reactions shown, namely inorganic Mn(IV) reduction by Fe(II) and Fe(III) reduction by organic matter (water-column DIR), represent two of the likely mechanisms for the development of depth gradients in carbonate alkalinity, $\delta^{13}C_{DIC}$, and increased activity of dissolved Mn (II) in shallow seawater. The schematic illustration of partial calcite preservation/replacement by ankerite and surrounding siderite, is based on observations from BSE image H of Fig. 3 (sample E1). The upward drop in the intensity of the blue gradient corresponds broadly to the postulated decline in the aqueous Fe/Mn ratio with decreasing water depth. See text for more details. (For interpretation of the references to colour in this figure legend, the reader is referred to the web version of this article.)

values in sample ARP1 are 1.2 and 3.5‰, respectively at 150 °C (Sheppard and Schwarcz, 1970; Golyshev et al., 1981). Complete conversion of one carbonate mineral to another in a closed system would not change $\delta^{13}C$ values. Ankerite, and especially siderite would have significantly higher $\delta^{13}C$ values than HMC were all three minerals to have formed at equilibrium. The siderite and ankerite have very similar $\delta^{13}C$ values which is consistent with bulk replacement of one by the other. The ankerite $\delta^{13}C$ values are on average 0.7‰ higher than those of HMC. This is consistent with a combination of equilibrium fractionation and bulk replacement of HMC by Fe-bearing carbonates. The similarity between ankerite and siderite $\delta^{13}C$ values (average difference 0.25‰) is nevertheless much more consistent with bulk replacement of ankerite by siderite than with equilibrium, where the difference in $\delta^{18}O$ should be as high as 3.5‰. The marginally higher $\delta^{13}C$ values for both iron carbonate phases compared to that of HMC, also suggest that any DIC potentially introduced from pore fluid would have to have been isotopically heavier in terms of carbon than the $\delta^{13}C$ value of HMC, a requirement that goes directly against processes of iron carbonate formation *via* organic matter remineralisation. The similarity in $\delta^{18}O$ values in the constituent carbonate minerals in ARP1 is also inconsistent with an influx of water from external sources becoming involved with the transformation of HMC to ankerite and siderite.

6. Conclusions and implications

The overarching scope of this work was to present a mineral-specific framework that can constrain the origin of carbonate minerals in IF and of the manganese typically associated with them. We reported consistent manganese enrichments in carbonate-rich IF samples well above crustal average across the top ~120 m of the Griquatown IF stratigraphy which – if interpreted in line with the oxygen whiff models – could conceivably translate into the most protracted period of pre-GOE oxygenation on record, if not the GOE itself. We critically reviewed the prevailing diagenetic model for IF, namely microbial DIR (and DMR, when Mn is implicated), which requires primary solid species in the form of Fe(III) oxyhydroxides, Mn(IV) oxides and organic matter in the precursor sediments. This model allows for no water-column reductive cycling of original Mn(IV) oxides and associated trace metals by, for example, abundant aqueous Fe(II) in the postulated stratified ferruginous ocean of that time. Additionally, co-precipitated organic carbon, metal oxyhydroxides and a variety of redox-sensitive trace metals theoretically associated with the latter, would have quantitatively reacted and sequestered in a closed diagenetic environment, in order to faithfully preserve primary marine isotopic signatures. These processes would have left no trace of the presumed primary mineralogy in the IF record, given the vanishingly low contents of organic carbon in IF (*e.g.*,

Dodd et al., 2019; Thompson et al., 2019); the striking lack of any preservation of Mn(IV) oxides in the rocks, combined with the presence of manganese almost exclusively in its divalent form in carbonate minerals (*e.g.,* Oonk et al., 2017); and the scarcity of hematite (at least in the rocks investigated here) as the closest possible proxy for primary ferric oxyhydroxide (ferrihydrite) precipitation.

It is our contention that current diagenetic models of biogenic carbonate formation and manganese uptake in IF and, by extension, the various geochemical and environmental interpretations based upon them, entail a large number of interlinked assumptions and pre-conditions which collectively render these models as unwieldy and somewhat contrived. We believe instead that primary, Fe/Mn-bearing HMC formation out of the oceanic water column as precursor to diagenetic ankerite and siderite formation, is by far the most parsimonious interpretation of the textural and chemical signatures we report in this paper. Our interpretation is also fully consistent with modern stratified lakes wherein low-$\delta^{13}C$ primary manganiferous carbonate formation coupled with organic matter and/or methane redox cycling, is documented (Havig et al., 2017; Herndon et al., 2018; Wittkop et al., 2020). It is also compatible with recently published research combining experimental work with observations in modern saline lacustrine environments, in which siderite can form *via* heated transformation (> 100 °C) of calcite and monohydrocalcite seeds in the presence of dissolved iron (Lin et al., 2019).

The implications of our interpretation have the potential to be far-reaching, especially with respect to the redox cycles of Mn, Fe and C during IF deposition, and their possible controls over the speciation behaviour of several redox-sensitive trace elements. Arguably the most profound implication is the elimination of DIR (and DMR, where relevant) as the dominant source of diagenetic carbonate alkalinity and Fe/Mn-carbonate formation, which would remove the necessity of exporting iron and manganese oxyhydroxides from the Neoarchaean-Palaeoproterozoic oceanic water column to the precursor IF sediment. Consequently, primary water-column formation of reduced Fe- and Mn-bearing phases (chiefly carbonates with specific reference to manganese) would be a more favourable alternative (see also Rasmussen et al., 2019; and Jiang and Tosca, 2019), thereby making carbonate minerals a suitable proxy for the geochemical characteristics and (traditional and non-traditional) stable isotope fractionation processes in the water mass in which they originally formed.

Our proposed interpretation is also in agreement with recent species-specific REE results from the same IF sequence which revealed the carbonate mineral fraction of the rocks as the one representing most faithfully the seawater signal during primary deposition (Oonk et al., 2018). Bulk-rock and carbonate-specific REE data record seawater-like patterns and consistently (albeit weakly) negative Ce anomalies, which have traditionally been interpreted as reflecting oxic marine conditions during primary chemical precipitation (*e.g.*, Bekker et al., 2010). In the modern oxygenated ocean, widespread Mn(IV) nodule/crust formation on the seafloor is known to act as powerful sink for Ce(IV), leading to strongly positive Ce anomalies in the latter and negative ones in contemporaneous seawater. Analogous interpretations for the Ce signal in IF are invariably challenged by the conspicuous lack of any positive Ce anomalies, irrespective of manganese content. This feature, combined with the overall paucity of Mn(IV) oxide preservation in the pre-GOE chemical sedimentary record, call for alternative explanations for the behaviour of Ce in early Precambrian seawater (see also Planavsky et al., 2010). Similarly, other mainstream interpretations of trace metal isotope systematics that require primary Fe(III) – and particularly Mn (IV) – oxyhydroxide deposition and therefore major paleoenvironmental and biological controls in redox potential (*e.g.,* oxygen whiffs), would also have to be critically reviewed.

An additional implication of our results concerns the broader issue of whether or not primary carbonate precipitation was occurring at all in the Precambrian ocean during IF deposition. It has been previously argued that the Archaean-Paleoproterozoic oceans would have contained high amounts of DIC (*e.g.,* Hotinski et al., 2004), a suggestion which is attractive in view of the elevated pCO_2 levels required in the Precambrian shallow ocean and atmosphere to offset the environmental effects of lower solar luminosity than today. However, traditional biological models of primary iron hydroxide precipitation *via* photoferrotrophy and subsequent diagenetic re-constitution into ferrous and mixed-valence assemblages *via* DIR, do not necessitate any primary precipitation of carbonate minerals out of seawater. Moreover, Fe(III) oxyhydroxide precipitation pathways, whether biological (*e.g.,* photoferrotrophy) or abiotic, are associated with relatively acidic conditions (see reaction (2) earlier and Fig. 9) which would naturally curtail marine carbonate formation and/or preservation.

Our results and interpretations demonstrate that a substantial component of the carbonate fraction of IF cannot be accounted for through classic models of bacterial reduction of oxyhydroxides of Fe (III) and – where applicable – Mn(III,IV). Specifically, the presence of relic HMC, abundance of ankerite and consistently measurable molar component of $MgCO_3$ in co-existing siderite, require that pathways of carbonate formation over and above (or instead of) those of DIR and DMR, would have to be invoked. This is consistent with the recent suggestion of Thompson et al. (2019) that approximately two-thirds of the carbonate budget preserved in IF would have to have originated from water-column carbonate formation, although the same authors do not constrain the exact mineralogical character of the postulated primary carbonate phases. Nevertheless, the intermediate $\delta^{13}C$ values of IF carbonate minerals between end-member organic and DIC values, naturally demand elevated contributions of seawater DIC to the CO_2 derived from the respiration of organic carbon, towards diagenetic carbonate formation. The above collectively converge to the notion that at least some primary carbonate formation out of seawater must have been operative. Our results, and particularly the documentation of HMC remnants containing variable yet appreciable Fe(II) and Mn(II) contents, indicate that such carbonates would also have been suitable primary precursors for later diagenetic replacement by ankerite and siderite in the presence of Fe(II)-rich pore fluids, thus negating the requirement for exclusively biological models of diagenetic Fe(+Mn) carbonate formation in IF.

Finally – and in a more local geological context – the high manganese abundances recorded in the uppermost Griquatown IF may potentially find direct chronostratigraphic correlatives in IF of the Koegas Subgroup (Schröder et al., 2011; Kendall et al., 2013; Warke et al., 2020b). The Koegas sequence of intercalated siliciclastic and chemical sediments – including IF of the Rooinekke and Nelani Formations (Schröder et al., 2011) – has traditionally been thought to be younger than the Griquatown IF. The latter contention has hinged in large part on previously proposed stratigraphic age relationships and interpretations, which incorrectly required a *ca.* 200 Ma hiatus to exist at the regional stratigraphic contact between the Griquatown IF and Makganyene Formation of, respectively, the uppermost Ghaap and basal Postmasburg Groups of the Transvaal Supergroup (Kopp et al., 2005; Gumsley et al., 2017). In the same context, high Mn in carbonates of the Koegas IF and associated Mo isotope fractionation effects have been interpreted as ultimate outcomes of an oxygen whiff (Kurzweil et al., 2016). Given the broadly comparable ages for the Koegas Subgroup and the Griquatown IF (Kendall et al., 2013; Gumsley et al., 2017; Lantink et al., 2019; Warke et al., 2020b) and the evidently conformable nature of the contact between the Griquatown IF and overlying Makganyene diamictite (Fig. 1B), we are inclined to interpret the source for the high Mn abundance in both the Koegas and upper Griquatown IF as having being potentially synchronous. This would place the two successions as lateral correlative facies, with the Koegas strata reflecting near-shore conditions characterised by mixed chemical-siliciclastic deposition, whereas the Griquatown IF would represent a more open pelagic and thus purely chemical depositional end-member. New and precise absolute age constraints for the Koegas and upper Griquatown IF may lend support to, or invalidate, the above interpretations.

Declaration of competing interest

The authors declare that they have no known competing financial interests or personal relationships that could have appeared to influence the work reported in this paper.

Acknowledgements

HT acknowledges generous funding by the company ASSMANG Ltd for the establishment of research unit PRIMOR at Rhodes University since 2014. The company SOUTH32 in Hotazel, and particularly Mr T. Rambuda and Mr E.P. Ferreira, are thanked for providing unconstrained access to all drillcores sampled for this study. PRDM acknowledges financial support from Rhodes University through the Hugh Kelly Visiting Fellowship for 2016. Sherissa Roopnarain (University of Cape Town) is gratefully acknowledged for assisting with the sequential carbonate stable isotope analyses. Constructive reviews by three anonymous reviewers assisted us greatly in making improvements to earlier versions of our manuscript.

Appendix A. Supplementary data

Supplementary data to this article can be found online at https://doi.org/10.1016/j.precamres.2020.105878.

References

Al-Aasm, I.S., Taylor, B.E., South, B., 1990. Stable isotope analysis of multiple carbonate samples using selective acid extraction. Chem. Geol. 80, 119–125.
Anbar, A.D., Holland, H.D., 1992. The photochemistry of manganese and the origin of banded iron formations. Geochim. Cosmochim. Acta 56, 2595–2603.
Anbar, A.D., Duan, Y., Lyons, T.W., Arnold, G.L., Kendall, B., Creaser, R.A., Kaufman, A.J., Gordon, G.W., Scott, C., Garvin, J., Buick, R., 2007. A Whiff of Oxygen before the Great Oxidation Event? Science 317, 1903–1906.
Baur, M.E., Hayes, J.M., Studley, S.A., Walter, M.R., 1985. Millimeter-scale variations of stable isotope abundances in carbonates from Banded Iron-Formations in the Hamersley Group of Western Australia. Econ. Geol. 80, 270–282.
Bekker, A., Slack, J.F., Planavsky, N., Krapez, B., Hofmann, A., Konhauser, K.O., Rouxel, O.J., 2010. Iron Formation: the sedimentary product of a complex interplay among mantle, tectonic, oceanic, and biospheric processes. Econ. Geol. 105, 467–508.
Beukes, N.J., Klein, C., 1990. Geochemistry and sedimentology of a facies transition - from microbanded to granular iron-formation - in the early Proterozoic Transvaal Supergroup, South Africa. Precambrian Res. 47, 99–139.
Crowe, S.A., Jones, C.A., Katsev, S., Magen, C., O'Neill, A.H., Sturm, A., Canfield, D.E., Haffner, G.D., Mucci, A., Sundby, B., Fowle, D.A., 2008. Photoferrotrophs thrive in an Archean Ocean analogue. Proc. Nat. Ac. Sci. 105, 15938–15943.
Dodd, M.S., Papineau, D., Pirajno, F., Wan, Y., Karhu, J.A., 2019. Minimal biomass deposition in banded iron formations inferred from organic matter and clay relationships. Nat. Commun. 10, 1–13.
Dromgoole, E.L., Walter, L.M., 1990. Iron and manganese incorporation into calcite: effects of growth kinetics, temperature and solution chemistry. Chem. Geol. 81, 311–336.
Fröelich, P.N., Klinkhammer, G.P., Bender, M.L., Luedtke, N.A., Heath, G.R., Cullen, D., Dauphin, P., Hammond, D., Hartman, B., Maynard, V., 1979. Early oxidation of organic matter in pelagic sediments of the eastern equatorial Atlantic: suboxic diagenesis. Geochim. Cosmochim. Acta 43, 1075–1090.
Gole, M.J., Klein, C., 1981. Banded Iron Formations through much of Precambrian time. J. Geol. 89, 169–183.
Golyshev, S.I., Padalko, N.L., Pechenkin, S.A., 1981. Fractionation of stable oxygen and carbon isotopes in carbonate systems. Geochem. Intern. 18, 85–99.
Gumsley, A.P., Chamberlain, K.R., Bleeker, W., Söderlund, U., de Kock, M.O., Larsson, E.R., Bekker, A., 2017. Timing and tempo of the Great Oxidation Event. Proc. Natl. Acad. Sci. 114, 1811–1816.
Haugaard, R., Pecoits, E., Lalonde, S., Rouxel, O., Konhauser, K.O., 2016. The Joffre banded iron formation, Hamersley Group, Western Australia: assessing the palaeoenvironment through detailed petrology and chemostratigraphy. Precambrian Res. 273, 12–37.
Havig, J.R., Hamilton, T.L., McCormick, M., McClure, B., Sowers, T., Wegter, B., Kump, L.R., 2017. Water column and sediment stable carbon isotope biogeochemistry of permanently redox-stratified Fayetteville Green Lake, New York, USA. Limnol. Oceanogr. 63, 570–587.
Heimann, A., Johnson, C.M., Beard, B.L., Valley, J.W., Roden, E.E., Spicuzza, M.J., Beukes, N.J., 2010. Fe, C, and O isotope compositions of banded iron formation carbonates demonstrate a major role for dissimilatory iron reduction in ~2.5 Ga marine environments. Earth Planet. Sci. Let. 294, 8–18.
Herndon, E.M., Havig, J.R., Singer, D.M., McCormick, M.L., Kump, L.R., 2018. Manganese and iron geochemistry in sediments underlying the redox-stratified Fayetteville Green Lake. Geochim. Cosmochim. Acta 231, 50–63.
Hoffman, P.F., 2013. The Great Oxidation and a Siderian snowball Earth: MIF-S based correlation of Paleoproterozoic glacial epochs. Chem. Geol. 362, 143–156.
Hotinski, R.M., Kump, L.R., Arthur, M.A., 2004. The effectiveness of the Paleoproterozoic biological pump: a $\delta^{13}C$ gradient from platform carbonates of the Pethei Group (Great Slave Lake Supergroup, NWT). Geol. Soc. Am. Bull. 116, 539–554.
Jiang, C.Z., Tosca, N.J., 2019. Fe(II)-carbonate precipitation kinetics and the chemistry of anoxic ferruginous seawater. Earth Planet. Sci. Let. 506, 231–242.
Johnson, C.M., Beard, B.L., Beukes, N.J., Klein, C., O'Leary, J.M., 2003. Ancient geochemical cycling in the Earth as inferred from Fe isotope studies of banded iron formations from the Transvaal Craton. Contrib. Mineral. Petrol. 144, 523–547.
Johnson, C.M., Roden, E.E., Welch, S.A., Beard, B.L., 2005. Experimental constraints on Fe isotope fractionation during magnetite and Fe carbonate formation coupled to dissimilatory hydrous ferric oxide reduction. Geochim. Cosmochim. Acta 69, 963–993.
Johnson, C.M., Ludois, J.M., Beard, B.L., Beukes, N.J., Heimann, A., 2013a. Iron formation carbonates: paleoceanographic proxy or recorder of microbial diagenesis? Geology 41, 1147–1150.
Johnson, J.E., Webb, S.M., Thomas, K., Ono, S., Kirschvink, J.L., Fischer, W.W., 2013b. Manganese-oxidizing photosynthesis before the rise of cyanobacteria. Proc. Nat. Ac. Sci. 110, 11238–11243.
Kaufman, A.J., Hayes, J.M., Klein, C., 1990. Primary and diagenetic controls of isotopic compositions of iron-formation carbonates. Geochim. Cosmochim. Acta 54, 3461–3473.
Kendall, B., Van Acken, D., Creaser, R.A., 2013. Depositional age of the early Paleoproterozoic Klipputs Member, Nelani Formation (Ghaap Group, Transvaal Supergroup, South Africa) and implications for low-level Re–Os geochronology and Paleoproterozoic global correlations. Precambrian Res. 237, 1–12.
Klein, C., 2005. Some Precambrian banded iron-formations (BIFs) from around the world: Their age, geologic setting, mineralogy, metamorphism, geochemistry, and origin. Am. Mineral. 90, 1473–1499.
Klein, C., Gole, M.J., 1981. Mineralogy and petrology of parts of the Marra Mamba Iron Formation, Hamersley Basin, Western Australia. Am. Mineral. 66, 507–525.
Konhauser, K.O., Hamade, T., Raiswell, R., Morris, R.C., Ferris, F.G., Southam, G., Canfield, D.E., 2002. Could bacteria have formed the Precambrian banded iron formations? Geology 30, 1079–1082.
Konhauser, K.O., Newman, D.K., Kappler, A., 2005. The potential significance of microbial Fe(III) reduction during deposition of Precambrian banded iron formations. Geobiology 3, 167–177.
Konhauser, K.O., Planavsky, N.J., Hardisty, D.S., Robbins, L.J., Warchola, T.J., Haugaard, R., Lalonde, S.V., Partin, C.A., Oonk, P.B.H., Tsikos, H., Lyons, T.W., Bekker, A., Johnson, C.M., 2017. Iron formations: a global record of Neoarchaean to Palaeoproterozoic environmental history. Earth Sci. Rev. 172, 140–177.
Kopp, R.E., Kirschvink, J.L., Hilburn, I.A., Nash, C.Z., 2005. The Paleoproterozoic snowball Earth: a climate disaster triggered by the evolution of oxygenic photosynthesis. Proc. Natl. Acad. Sci. 102, 11131–11136.
Kurzweil, F., Wille, M., Gantert, N., Beukes, N.J., Schoenberg, R., 2016. Manganese oxide shuttling in pre-GOE oceans – evidence from molybdenum and iron isotopes. Earth Planet. Sci. Let. 452, 69–78.
Lantink, M.L., Davies, J.F.H.L., Mason, P.R.D., Schaltegger, U., Hilgen, F.J., 2019. Climate control on banded iron formations linked to orbital eccentricity. Nat. Geosci. 12, 369–374.
Lin, C.Y., Turchyn, A.V., Krylov, A., Antler, G., 2019. The microbially driven formation of siderite in salt marsh sediments. Geobiology 18. https://doi.org/10.1111/gbi.12371.
Myers, C.R., Nealson, K.H., 1988. Bacterial manganese reduction and growth with manganese oxide as the sole electron acceptor. Science 240, 1319–1321.
Nealson, K.H., Myers, C.R., 1990. Iron reduction by bacteria: a potential role in the genesis of banded iron formations. Am. J. Sci. 290, 35–45.
Oonk, P.B.H., 2017. Species-specific trace element and stable isotope geochemistry across the BIF stratigraphy of the Transvaal Supergroup in Griqualand West, South Africa, and implications for the history of atmospheric oxygen. PhD thesis, 211 pages.
Oonk, P.B.H., Tsikos, H., Mason, P.R.D., Henkel, S., Staubwasser, M., Fryer, L., Poulton, S.W., Williams, H.M., 2017. Fraction-specific controls on the trace element distribution in iron formations: Implications for trace metal stable isotope proxies. Chem. Geol. 474, 17–32.
Oonk, P.B.H., Mason, P.R.D., Tsikos, H., Bau, M., 2018. Fraction-specific rare earth elements enable the reconstruction of primary seawater signatures from iron formations. Geochim. Cosmochim. Acta 238, 102–122.
Ostrander, C.M., Nielsen, S.G., Owens, J.D., Kendall, B., Gordon, G.W., Romaniello, S.J., Anbar, A.D., 2019. Fully oxygenated water columns over continental shelves before the great oxidation event. Nat. Geosci. 12, 186–191.
Planavsky, N., Bekker, A., Rouxel, O.J., Kamber, B., Hofmann, A., Knudsen, A., Lyons, T.W., 2010. Rare Earth Element and yttrium compositions of Archean and Paleoproterozoic Fe formations revisited: New perspectives on the significance and mechanisms of deposition. Geochim. Cosmochim. Acta 74, 6387–6405.
Planavsky, N., Asael, D., Hofmann, A., Reinhard, T., Lalonde, S.V., Knudsen, A., Wang, X., Ossa Ossa, F., Pecoits, E., Smith, A.J.B., Beukes, N.J., Bekker, A., Johnson, T.M., Konhauser, K.O., Lyons, T.W., Rouxel, O.J., 2014. Evidence for oxygenic photosynthesis half a billion years before the Great Oxidation Event. Nat. Geosci. 7, 283–286.
Posth, N.R., Köhler, I., Swanner, D.E., Schröder, C., Wellmann, E., Binder, B., Konhauser, K.O., Neumann, U., Berthold, C., Nowak, M., Kappler, A., 2013. Simulating Precambrian banded iron formation diagenesis. Chem. Geol. 362, 66–73.
Rasmussen, B., Muhling, J.R., Tosca, N.J., Tsikos, H., 2019. Evidence for anoxic shallow oceans at 2.45 Ga: Implications for the rise of oxygenic photosynthesis. Geology 47, 622–626.

Schröder, S., Bedorf, D., Beukes, N.J., Gutzmer, J., 2011. From BIF to red beds: Sedimentology and sequence stratigraphy of the Paleoproterozoic Koegas Subgroup (South Africa). Sediment. Geol. 236, 25–44.

Sheppard, S.M.F., Schwarcz, H.P., 1970. Fractionation of carbon and oxygen isotopes and magnesium between coexisting metamorphic calcite and dolomite. Contrib. Mineral. Petrol. 26, 161–198.

Swanner, E.D., Planavsky, N.J., Lalonde, S.V., Robbins, L.J., Bekker, A., Rouxel, O.J., Saito, M.A., Kappler, A., Mojzsis, S.J., Konhauser, K.O., 2014. Cobalt and marine redox evolution. Earth Planet. Sci. Let. 390, 253–263.

Swanner, E.D., Maisch, M., Wu, W., Kappler, A., 2018. Oxic Fe(III) reduction could have generated Fe(II) in the photic zone of Precambrian seawater. Sci. Rep. 8. https://doi.org/10.1038/s41598-018-22694-y.

Thibon, F., Blichert-Toft, J., Albarede, F., Foden, J., Tsikos, H., 2019. A critical evaluation of copper isotopes in Precambrian iron formations as a paleoceanographic proxy. Geochim. Cosmochim. Acta 264, 130–140.

Thompson, K.J., Kenward, P.A., Bauer, K.W., Warchola, T., Gauger, T., Martinez, R., Simister, R.L., Michiels, C.C., Llirós, M., Reinhard, C.T., Kappler, A., Konhauser, K.O., Crowe, S.A., 2019. Photoferrotrophy, deposition of banded iron formations, and methane production in Archean oceans. Sci. Adv. 5 (11). https://doi.org/10.1126/sciadv.aav2869.

Tsikos, H., Moore, J.M., 1997. Petrography and geochemistry of the Paleoproterozoic Hotazel Iron-Formation, Kalahari manganese field, South Africa; implications for Precambrian manganese metallogenesis. Econ. Geol. 92, 87–97.

Tsikos, H., Beukes, N.J., Moore, J.M., Harris, C., 2003. Deposition, diagenesis, and secondary enrichment of metals in the Paleoproterozoic Hotazel Iron Formation, Kalahari manganese field, South Africa. Econ. Geol. 98, 1449–1462.

Tsikos, H., Matthews, A., Erel, Y., Moore, J.M., 2010. Iron isotopes constrain biogeochemical redox cycling of iron and manganese in a Palaeoproterozoic stratified basin. Earth Planet. Sci. Lett. 298, 125–134.

Walker, J.C.G., 1984. Suboxic diagenesis in banded iron formations. Nature 309, 340–342.

Warke, M.R., Di Rocco, T., Zerkle, A.L., Lepland, A., Prave, A.R., Martin, A.P., Ueno, Y., Condon, D.J., Claire, M.W., 2020a. The Great Oxidation Event preceded a Paleoproterozoic "snowball Earth". Proc. Natl. Acad Sci. 202003090. https://doi.org/10.1073/pnas.200309011.

Warke, M.R., Strauss, H., Schröder, S., 2020b. Positive cerium anomalies imply pre-GOE redox stratification and manganese oxidation in Paleoproterozoic shallow marine environments. Prec. Res. 344, 105767.

Wittkop, C., Swanner, E.D., Grengs, A., Lambrecht, N., Fakhraee, M., Myrbod, A., Bray, A.W., Poulton, S.W., Katsev, S., 2020. Evaluating a primary carbonate pathway for manganese enrichments in reducing environments. Earth Planet. Sci. Let. 538. https://doi.org/10.1016/j.Earth Planet. Sci. Let. 2020.116201.